International Journal of Applied Chemistry.
ISSN 0973-1792 Volume 12, Number 2 (2016) pp. 139-156

http://www.ripublication.com

Void Coalescence and Texture Analysis of Various Indian Stainless Steel Sheets Formed Under Different Stress Conditions

K Pandian[1]* and Dr K Manonmani[2]

*[1]*Dy.General Manager, Central Marketing Organization,*
Steel Authority of India Ltd. E-mail: salempandian@gmail.com
[2] Associate Professor, Dept of Mechanical Engg, GCT, Coimbatore, Tamilnadu.
E-mail: manokmani@yahoo.co.in

Abstract

Formability, an important mechanical property of the sheet metal is strongly reliant on the crystallographic texture**.** This paper deals with the perspective of crystallographic texture, void coalescence and its relevance with the formability of different Indian stainless steel grades, namely, SS301, SS304, SS430, SS409M, and low nickel austenitic grade stainless steel(SSLN1)**.** Forming limit diagrams were determined and plotted experimentally**.** Further their bulk X-ray crystallographic textures and their ODF plots were analyzed**.** The forming limit diagrams of different Indian stainless steel grades were examined with respect to the crystallographic texture point of view**.** The forming limit diagrams and crystallographic textures were then correlated with normal anisotropy of the sheet metal and it is further correlated with the void coalescence parameters**.** It is observed that the formability of SSLN1 is comparable with SS304**.**

Keywords: Forming; Plastic behavior; Fractography, Crystallography Texture.

Nomenclature

ε_1	Major strain
ε_2	Minor strain
ε_3	Thickness strain
ε_e	Effective strain
ε_m	Hydrostatic or mean strain

γ_{12}, γ_{23} and γ_{13}	Mohr's circle shear strains (the subscripts 1, 2 & 3 represent major, minor and thickness strains)
δ_d	Ligament thickness
d-factor	Ratio of δ_d to radius of void
T	Stress triaxiality factor or ratio
σ_e	Effective stress
σ_m	Mean or hydrostatic stress
R	Plastic strain ratio
n	Stain hardening exponent
K	Strength coefficient
R_{av}	Average plastic strain ratio or normal anisotropy = $(R_0 + R_{90} + 2R_{45})/4$
n_{av}	Average strain hardening index = $(n_0 + n_{90} + 2n_{45})/4$

INTRODUCTION

Stainless steel is a commonly available material possessing good corrosion resistance and elevated carbon to allow for cold working to a variety of tempers. It can be obtained in the annealed, 1/4 hard, 1/2 hard, 3/4 hard, full hard, and extra full hard and high yield tempers. Usually SS304 is used for the manufacturing of household utensils. SS409M grade stainless steel is mostly used in the production of railway wagons in India. SS430 is ferritic chromium steel, resistant to atmospheric corrosion and fresh water used in landscaping. SS301 have poor application compared to SS304 because of higher carbon content. Since the cost of nickel is very high, SS304 grade is unaffordable for the manufacturing of utensils. Alternatively, low nickel stainless steel sheets (SSLN1) are developed as a substitute for manufacturing of utensils at affordable cost. This is developed by Steel Authority of India, Salem Steel Plant, Salem, Tamil Nadu, India.

In any material, fracture occurs due to the nucleation, growth and coalescence of voids formed after the onset of necking. Therefore the nucleation, growth and coalescence of voids influence the fracture behavior of any material. The voids are spherical in materials and remain spherical in growth, but many engineering materials have non spherical voids. Critical void volume fraction was often used to designate the final material failure. **Gurson[1]** in 1977 first studied the theory of ductile rupture through void nucleation growth and developed gurson model which is widely used afterwards. The forming limit diagram (FLD) enables the prediction of deformation that can lead to the failure of the material for different strain paths and are considered as an important tool in the die design as well as to optimize and correct problems in the line production as described by **William Hosford et al. [2]. Narayanasamy et al. [3]** tested different materials and from strain based limit diagrams, the stress based forming and fracture limit diagrams were drawn. **Benzerga et al. [4]** concluded that the particle volume fraction, aspect ratios and relative spacing affects nucleation, growth and coalescence of voids. Nucleation, growth and coalescence of voids formed after the onset of necking are influenced greatly by the microstructure. **Ragab**

et al. [5] observed that experimentally determined values of initial void volume fraction together with a reasonable thickness imperfection appeared to give better forming limit diagram. Also a model for predicting FLD adopting the heterogeneous distribution of voids within the sheet metal and their growth with straining was proposed. **Gao et al. [6]** observed that the critical strain at the onset of void coalescence depends on material flow properties, microstructural properties and the stress state. The stress parameters, namely, the stress and strain triaxiality ratios can be used to characterize the effect of the macroscopic stress state on the void growth and coalescence process in the representative material volume (RMV). **Bandstra et al. [7]** observed that a void coalescence criterion depends strongly on strain hardening and void growth that initially occurs at a rate close to that predicted for an isolated void. **Li et al. [8]** studied the effects of yield strength gradients (YSG) on the void growth and coalescence in the graded matrix materials by use of an axisymmetric cell model and concluded that the critical effective strain has close relation with the YSGs in the matrix materials and also the YSG distribution of matrix has a visible effect on the critical void volume fraction. **Ragab [9]** studied the effect of strain hardening void shape, size and aspect ratio and also developed a analytical model to predict the void parameters. **Monchiet et al. [10]** studied yield criteria for anisotropic metals with prolate or oblate voids. **Niordson [11]** studied void growth to coalescence in a non-local material and showed that the suppression of void growth on the micron scale that leads to larger attainable stress levels when compared to predictions of conventional theory, as well as a delay in the onset of localization which gives rise to a more ductile material behavior. **Hucthison [12]** studied the effect of initial void shape on the occurrence of cavitation instability in elastic and plastic solids. **Kanni Raj et al. [13]** studied the formability of metastable low nickel austenitic stainless steel sheets. **Hutchinson et al. [14]** studied texture in hot rolled austenite and resulting transformation products both nucleation and growth are considered to play roles in defining transformation textures, depending on the physical processes which are involved. **Safaeirad et al. [15]** studied the effect of microstructure and texture on formability and mechanical properties of hot-dip galvanized steel sheets. **Samajdar et al. [16]** studied development of recrystallization texture in IF-steel as an effort to explain developments in global texture from microtextural studies. **Samajdar et al. [17]** studied cube recrystallization texture in warm deformed aluminum. Evaluation of formability and planar anisotropy based on textures in aluminum alloys processed by a shear deforming process was done by **Hana et al. [18]**.

The present work deals with void coalescence, crystallographic texture and its relevance with the formability of different Indian stainless steel grades, namely, SS301, SS304, SS430, SS409M, and low nickel austenitic grade stainless steels(SSLN1). Forming limit diagrams of the aforesaid different Indian stainless steel grades were established based on the experimental results. Further FLDs and crystallographic textures were correlated with normal anisotropy of the sheet metal and the void coalescence parameters.

EXPERIMENTAL WORK

Metallography

In order to study the microstructure the cut samples of different stainless steel sheets were mounted by cold setting for easy handling.

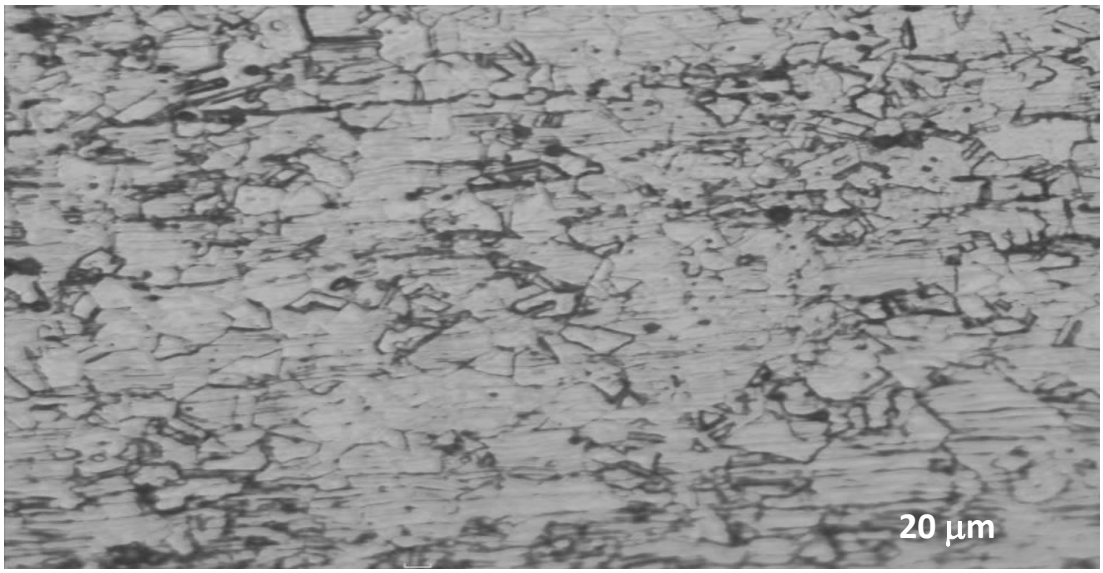

Figure 1a: Optical micrographs of SS304 grade Stainless Steel

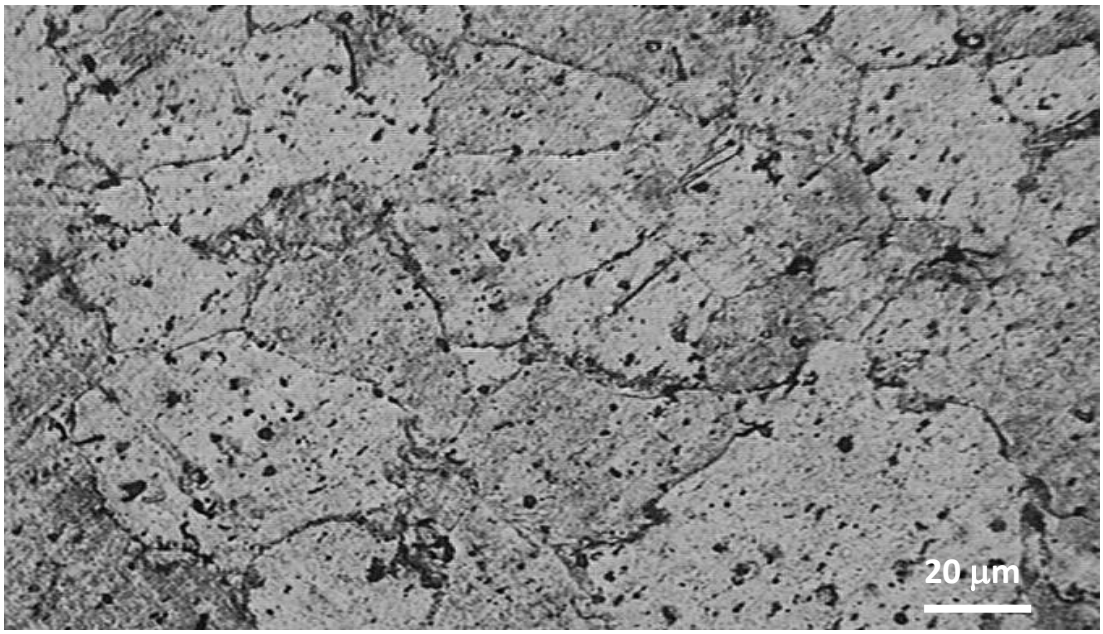

Figure 1b: Optical micrographs of SS430 grade of Stainless Steel

Using different emery paper polishing followed by polishing with diamond paste the mirror finished surface was obtained. After polishing the samples microstructural characterization was performed using optical microscope. The microstructures of the studied steels were revealed by chemical etching with 10% oxalic acid, glyceregia and 5% nital as shown in **Figures 1a & 1b**.

Forming limit diagram

The tensile properties of the five different Indian stainless steel grades supplied by Salem Steel Plant, Salem, Tamil Nadu, India were determined using Hounsfield Tensometer. Using a double action hydraulic press of 2000 kN capacity with standard die and punch set up used for formability tests, sheet samples of 300mm length with different widths, namely, 100, 120, 140, 160, 180, 200 and 220mm were formed up to fracture to vary the strain conditions and to study the void formation under different conditions. Circular grids in rectangular array pattern were printed on the surface of the sheet blanks earlier to forming. After deformation the aforesaid printed circles became elliptical in shape because of different strain conditions. The major diameter and minor diameter of these ellipses were used to determine the major strain (e_1) and minor strain (e_2). The formulae used to calculate these strains are given as follows as explained by **Narayanasamy and Sathiya Narayanan [3]**,

$$\text{Major strain } (\varepsilon_1) = \ln\left(\frac{\text{Major diameter of the ellipse}}{\text{Original diameter of the circle}}\right)$$

$$\text{Minor strain } (\varepsilon_2) = \ln\left(\frac{\text{Minor diameter of the ellipse}}{\text{Original diameter of the circle}}\right)$$

The thickness of the sheet in different locations were measured and thickness strain was calculated using the expression as explained **Narayanasamy and Sathiya Narayanan [3],**

$$\text{Thickness strain } (\varepsilon_3) = \ln\left(\frac{\text{Thickness after forming}}{\text{Original thickness}}\right)$$

All these strains ($\varepsilon_1, \varepsilon_2$ and ε_3) were measured in necked, fractured and safe regions. Using the measured strain values, the forming limit diagrams were plotted. Using the expressions provided in the **Ref. [19]**, the hydrostatic or mean strain and the effective strain can be determined.

Void Analysis

For void analysis fractured surfaces were observed for voids using a Scanning Electron Microscope (SEM) model JSM-5610LV. Using AutoCAD software, the size,

shape and perimeter of the voids were analyzed by importing the SEM images. Also, the relative spacing of the ligaments (dd) present between the two consecutive voids was also measured from the SEM images. The d-factor was then determined by dividing the relative spacing of the ligaments (dd) present between the two consecutive voids by the average radii of the voids which were derived from the measured void perimeters. For the prolate and oblate voids, the length and width of the voids were measured from the SEM images and then the length to width ratio (L/W) of the voids was calculated. A representative material area (RMA) was chosen and the total area of the voids present in this particular RMA was calculated as shown in **Figure 2**. From these data, the void area fraction, ratio of total area of the voids to the RMA was calculated **[19]**.

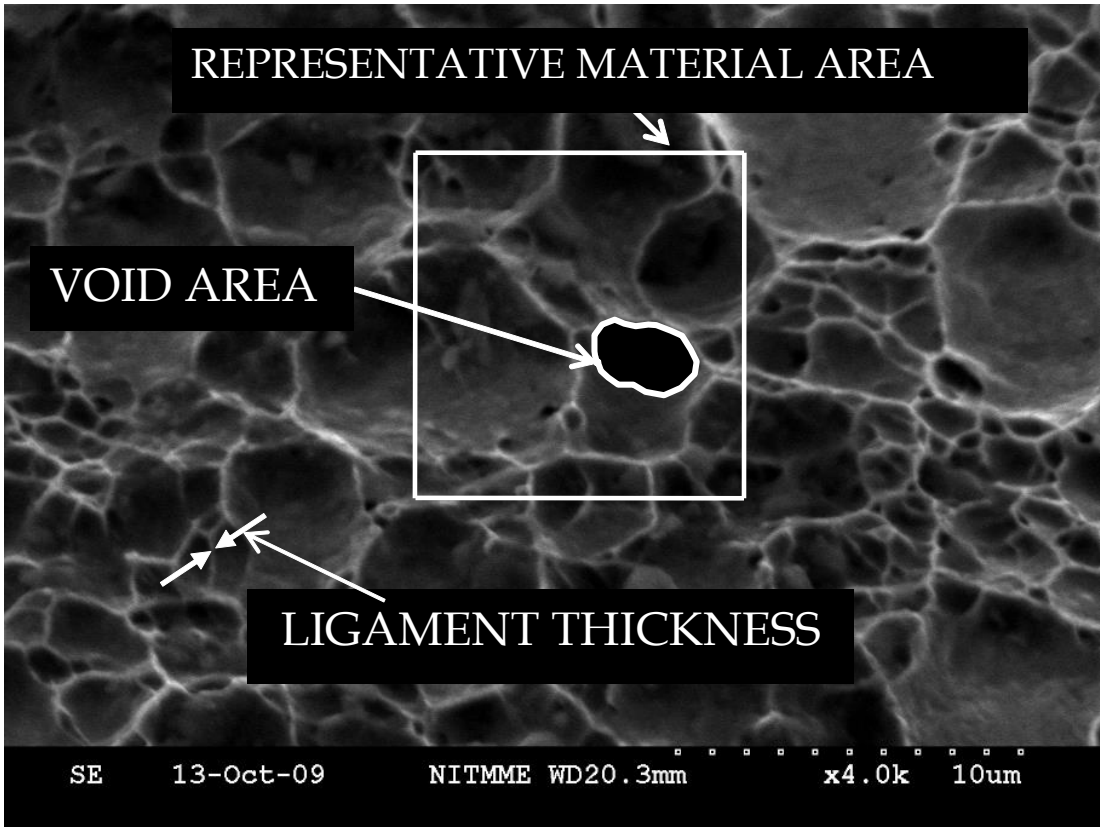

Figure 2: Schematic of void coalescence analysis

Texture Analysis

By inversion of four incomplete pole figures, texture measurements were obtained. X-ray Orientation Distribution Functions (ODFs) were calculated by standard series expansion method using the program MTM–FHM. Volume fractions, for individual texture and fibre components, were estimated by convoluting the X-ray ODFs (Orientation Distribution Function) with suitable model functions, with an integrated

ODF value of 1 and 16.5 Gaussian spread. The relative intensities of gamma and alpha fibre were computed from respective ODFs.

RESULTS AND DISCUSSION

Chemical Composition

The chemical composition of the stainless steel sheets supplied by M/s Salem Steel Plant, Steel Authority of India Limited (SAIL), Salem, Tamil Nadu, India is provided in **Table-1**. The chemical composition of SS301 has comparatively more amount of carbon compared with the other steels. SS301 derives its strength by the presence of carbide which is very hard in nature. The chemical composition of SS304 steel shows lesser amount of carbon, which means the amount of carbides present are comparatively lesser than SS301 and SS409M. The amount of nickel also affects the strength of steel with out increasing the brittleness. Among the steels tested, SS304 has the maximum amount of nickel and SS430 has the least amount of nickel. In stainless steel SSLN1, manganese is present in a considerable amount, which may lead to the formation of some second phase particles like manganese sulphide (MnS).

Table 1: Composition of stainless steels

Material	Thickness in mm	C	Cr	Ni	Mn	Si	S
SS301	1.2	0.150	17.0	7.00	2.00	1.00	0.030
SS304	1.2	0.055	18.2	8.10	8.10	0.35	0.001
SS409M	1.2	0.08	11.1	0.50	1.00	1.00	0.030
SS430	1.2	0.040	16.3	0.20	0.45	0.40	-
SSLN1	1.2	0.055	18.2	1.25	8.60	0.35	0.001

Microstructure

Stainless steel SS304 has a combination of fine and coarse network of austenitic grains. This has mixed grains. Twin bands can also be seen in the microstructure. In the case of SS301 it has coarse austenitic grains with carbides. As the carbon content is high in the case of SS301, there is a possibility for the formation of carbides. In the case of SSLN1, it has a combination of a network of fine and coarse austenitic grains. Whereas in the case of SS409M it has martensitic microstructure. SS430 has a coarse network of ferritic grains.

Tensile Properties

The average strain hardening exponent (n_{av}) value affects the stretchability and formability of the material. The tensile properties of the various stainless steels tested. It was observed that as the n_{av}-value increases, the stretchability increases. The SS304 sheet possesses comparatively a lower average strength coefficient value (K). Whereas SS301 and SSLN1 possess higher average strength coefficient value when compared to SS304, SS409M and SS430. The SS301 steel possesses a higher Value of ultimate tensile strength (UTS) compared to other two sheets and SS304 steel

possesses a lower yield stress compared to other sheets tested. The lower yield stress of the steel favours an early setup of plastic deformation during forming.

Limit Strains

The forming and fracture limit diagrams of all the stainless steel sheets tested are presented in **Figure 3a & 3b**.

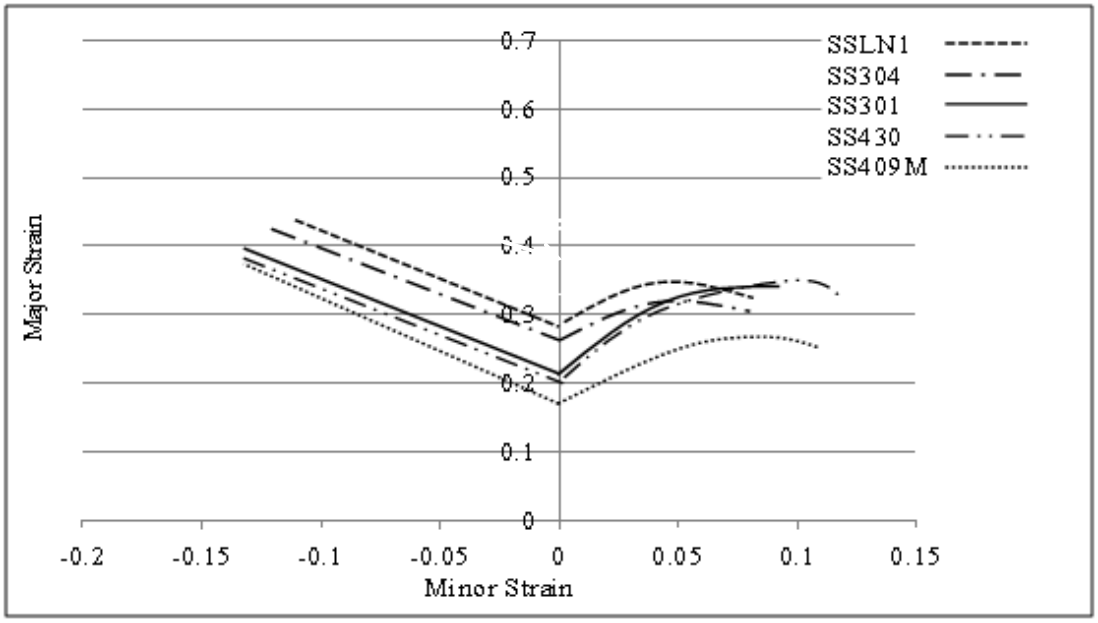

Figure 3a: Forming Limit Curves for various Stainless steels

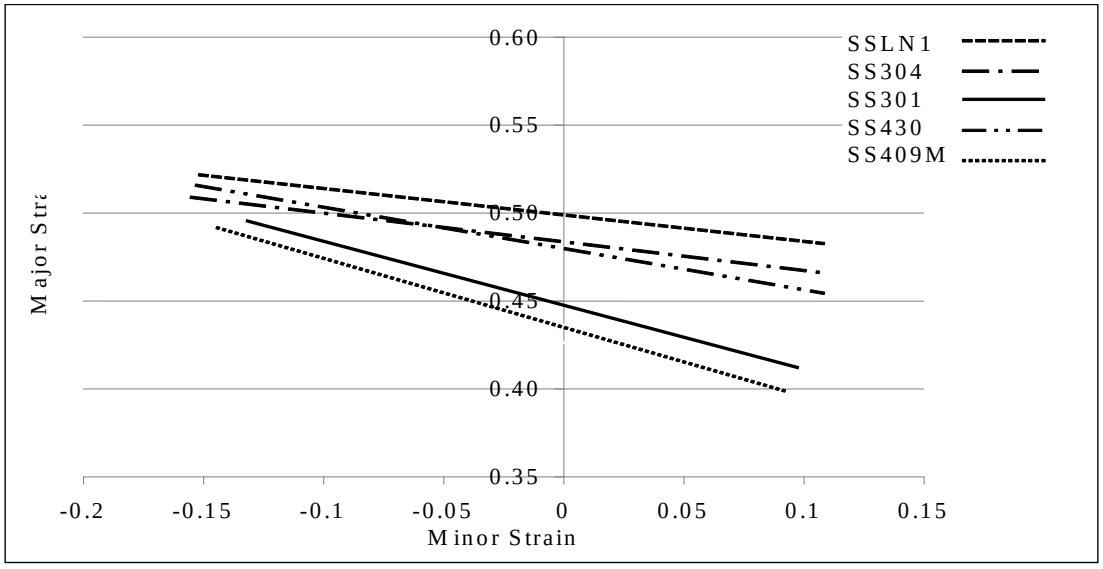

Figure 3b: Fracture Limit Curves for various Stainless steels

In the forming and fracture limit curves the dip in the central region of the curves corresponds to plane strain deformation. In the right hand side of the strain curve, in the tension–compression region, the strain is more due to the accommodation of more plastic deformation, whereas the left hand side of the strain curve represents the tension–tension region, where the strain is comparatively lesser due to lesser formability.

The diagonal shift of the forming and fracture limit curve of SSLN1 and SS304 steel sheets are similar and show that it accommodates more strain and better formability as compared to other stainless steel sheets tested. The formability of SS301 is poor compared to SSLN1 and SS304. Among the austenitic stainless steels SSLN1 shows better formability in all regions, namely, plain strain, tension-tension and tension-compression. SS409M shows poor formability due to the pressure of martensitic microstructure. The formability of SS430 is poor compared to austenitic stainless steels and better than SS409M. From the fracture limit curve, it is clear that the forming behaviour of SS409M is better in tension-compression region than tension-tension region. The above formability is comparable with other austenitic grades.

SEM Analysis

Figure 4 shows one of the SEM fractography of the different stainless steel sheets. Generally, the shape of the voids can be categorized as spherical, prolate and oblate voids. In the initial stage of research on voids, they are assumed spherical. Later, it is found that the shape of the voids is taking different shapes depending on the state of stress/strain conditions. The prolate and oblate voids are elliptical in shape.

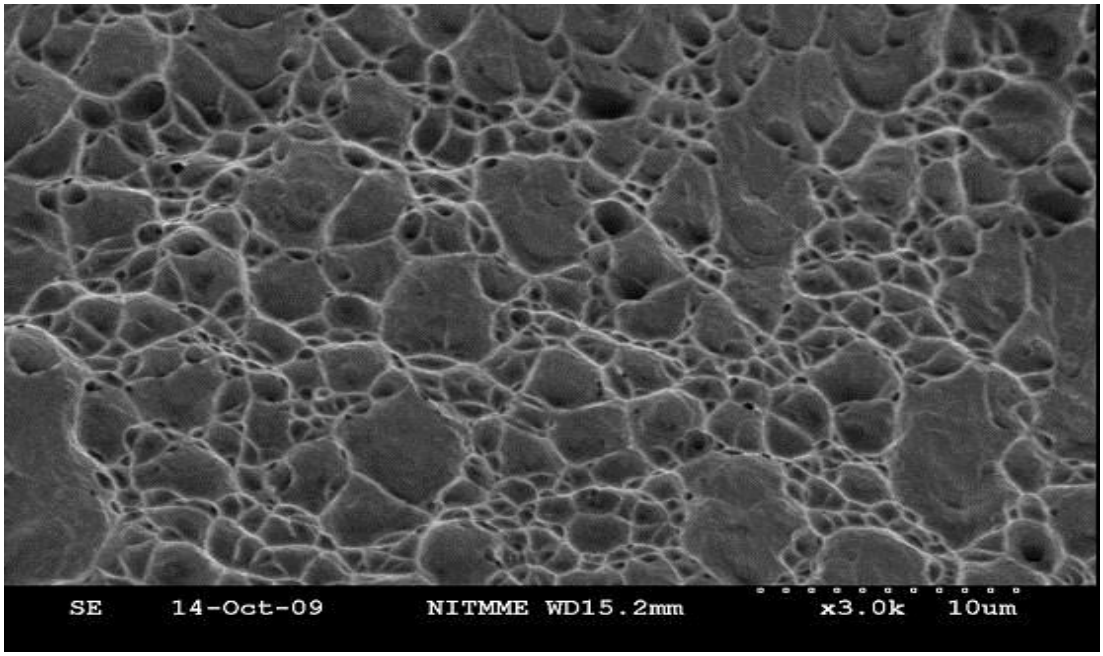

Figure 4: SEM image for the fracture surfaces of SS301: tension–compression condition

The prolate voids are elongated more in the thickness direction than in the plane of the sheet and the oblate voids are elongated more in the direction of plane of the sheet **[1]**. Not only the type of voids, but also the number of voids is affected by the forming conditions. Among the sheets taken for the study, the SS301 steel sheet shows large number of voids in the SEM images taken at its fracture surface compared to other steel sheets. The presence of large number of voids is due to the presence of more carbide particles. As the strain hardening index (n) value increases, the strain required for the plastic deformation also increases and this may be due to phase transformation which converts austenite to plastically strain induced martensite **[20, 21]**. Due to the presence of carbides in SS301, some facets (brittle fracture) can be seen in the SEM micrographs of tension-tension region.

In other sheets, the number of voids is least compared to SS304 sheet. It is also noticed that the voids are almost spherical in the case of the blanks of width 200 mm which is subjected to nearly equibiaxial strain condition. This is due to the reason that the major strain and minor strain are tensile in nature, they are acting in the plane of the surface of the sheet and the thickness strain is found to be lesser at fracture. In tension–compression strain condition, the minor strain (in the width direction) is less and therefore it shows smaller number of prolate voids. It is also true that the orientation of second phase particle influence the formation of both prolate and oblate voids.

These voids are formed around the second phase particle due to the mismatch of these second phase particles and the metal matrix, whereas in tension–tension strain condition, the voids are developed at the fracture of second phase particles and therefore they are in spherical shape. In the case of SSLN1, it has a combination of both smaller and bigger size dimples. This shows that the second phase particle present in the steel is not uniform in size. In the case of tension-tension region, the voids appear in elongated fashion. In this steel some areas of facets can be seen in the tension-tension region due to brittle behaviour compared to tension-compression region.

In the case of SS430, it has deep dimples with the larger area of facets. This shows that austenitic SS304 or SSLN1 is more ductile in nature than SS430. In the case of tension-tension region, facets area can be very clearly seen which exhibit brittleness compared to austenitic stainless steels. In SS409M, very large area of facet is due to the presence of martensite in the microstructure. In the case of tension-tension region, larger sized dimples can be seen.

Void Parameters

Figure 5 is plotted between the strain triaxiality factor (which is the ratio between hydrostatic strain and effective strain) and d-factor.

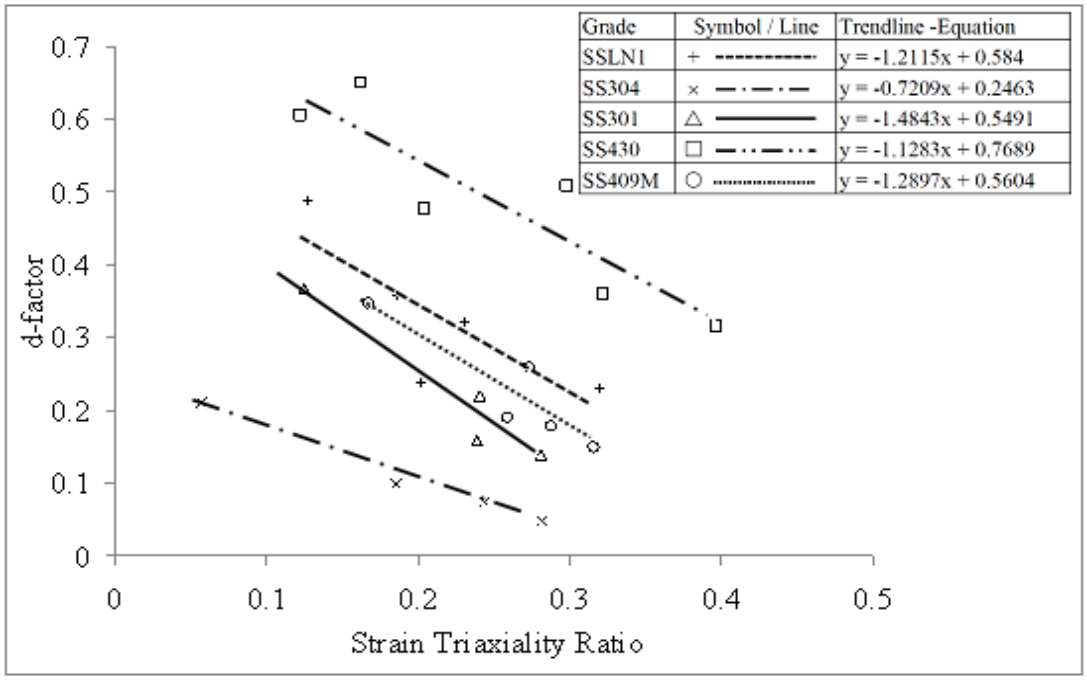

Figure 5: "d-factor" versus strain triaxiality factor (T_0) for stainless steel

From this figure, it is known that the effective strain increases as the void size decreases. Therefore it can be concluded that as the strain triaxiality factor increases the d-factor also increases. Austenitic stainless steels exhibit lower ligament thickness because the fracture behaviour of austenitic stainless steels is different compared to ferritic or martensitic stainless steels. Therefore, d-factor value decreases for austenitic stainless steels and is found to be the lowest. Further the strain-hardening index value is found to be higher for austenitic stainless steels because of phase transformation during plastic deformation which increases the formability. It is very difficult to compare with formability and d-factor in the case of austenitic stainless steels unlike in plain carbon steels. The ligament thickness value for SS430 and SS409M is found to be higher compared with austenitic stainless steels. Therefore, the d-factor value for SS430 and SS409M steels increases.

The behaviour of the δd -factor with mean strain is almost similar as in the previous case. The SS304 sheet shows lower slope value and therefore this sheet exhibits better formability. The strain triaxiality factor is responsible for the initiation of void and hydrostatic strain is responsible for the growth of the void.

Therefore, these two parameters have some impact on the void area fraction as well as on the formability. It shows that the fracture occurs when this void area fraction reaches a critical value for steels and for any given condition. This critical value also depends on the thickness of the sheet.

The nature of variation of void area fraction with respect to strain triaxiality factor shows the similar pattern but with different slope values. The hydrostatic stress and

the stress triaxiality factor are directly proportional to hydrostatic strain and strain triaxiality factors. Hence, the influence of hydrostatic stress and the stress triaxiality factor on δd-factor are assumed to be similar to that of hydrostatic strain and strain triaxiality factor.

The combination of lesser stress triaxiality factor (T) and higher Lode angle refers to higher severity of triaxial stress. The stress triaxiality and Lode angle parameters were determined as described elsewhere **[19]**. For the sheet metals subjected to tension–tension strain condition, the Lode angle is measured as a higher value and a lower value for tension–compression strain condition.

The higher Lode angle refers to higher severity of triaxial stress state. Therefore the severity of triaxial stress state is high for tension–tension strain condition and this shows lesser formability compared to tension–compression strain condition in all steels. In tension–tension strain condition, the d-factor and dd-factor have a lower value due to this higher Severity of triaxiality in all steels. In the case of SS430, both stress and strain triaxiality ratios increase due to the presence of deeper voids. The behaviour of SSLN1, SS304 and SS301 (austenitic grades) are almost the same. In the case of SS409M stress triaxiality ratio is very high compared to austenitic grades. Therefore, austenitic stainless steels show better formability than ferritic and martensitic stainless steel grades.

From **Figure 6,** the SS301 sheet shows the highest L/W ratio compared to other steels for any given minor strain value. The SS304 steel shows the lowest L/W ratio and exhibits better formability. SS430 shows lower value of L/W ratio compared to other steels.

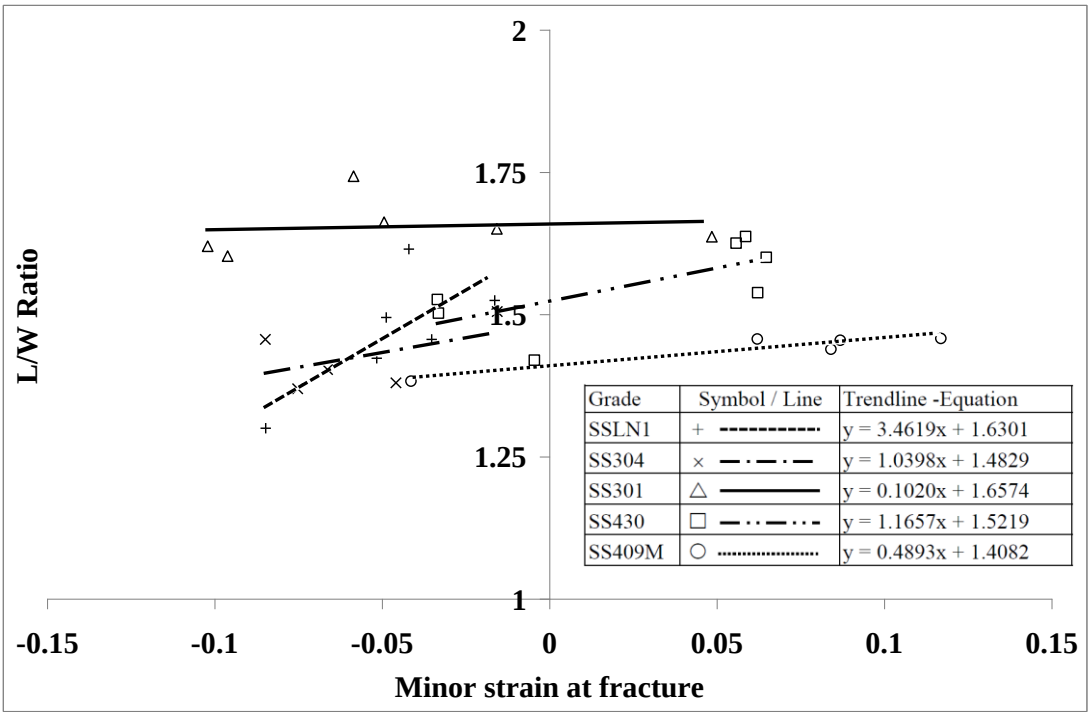

Figure: 6 L/W Ratio versus strain Minor Strain at Fracture for stainless steel

Texture analysis

The ODF plots and the pole figures obtained from X-ray texture measurements are shown in **Figure 7a and 7b**, as pole figures and ODFs for FCC and BCC stainless sheet of different grades.

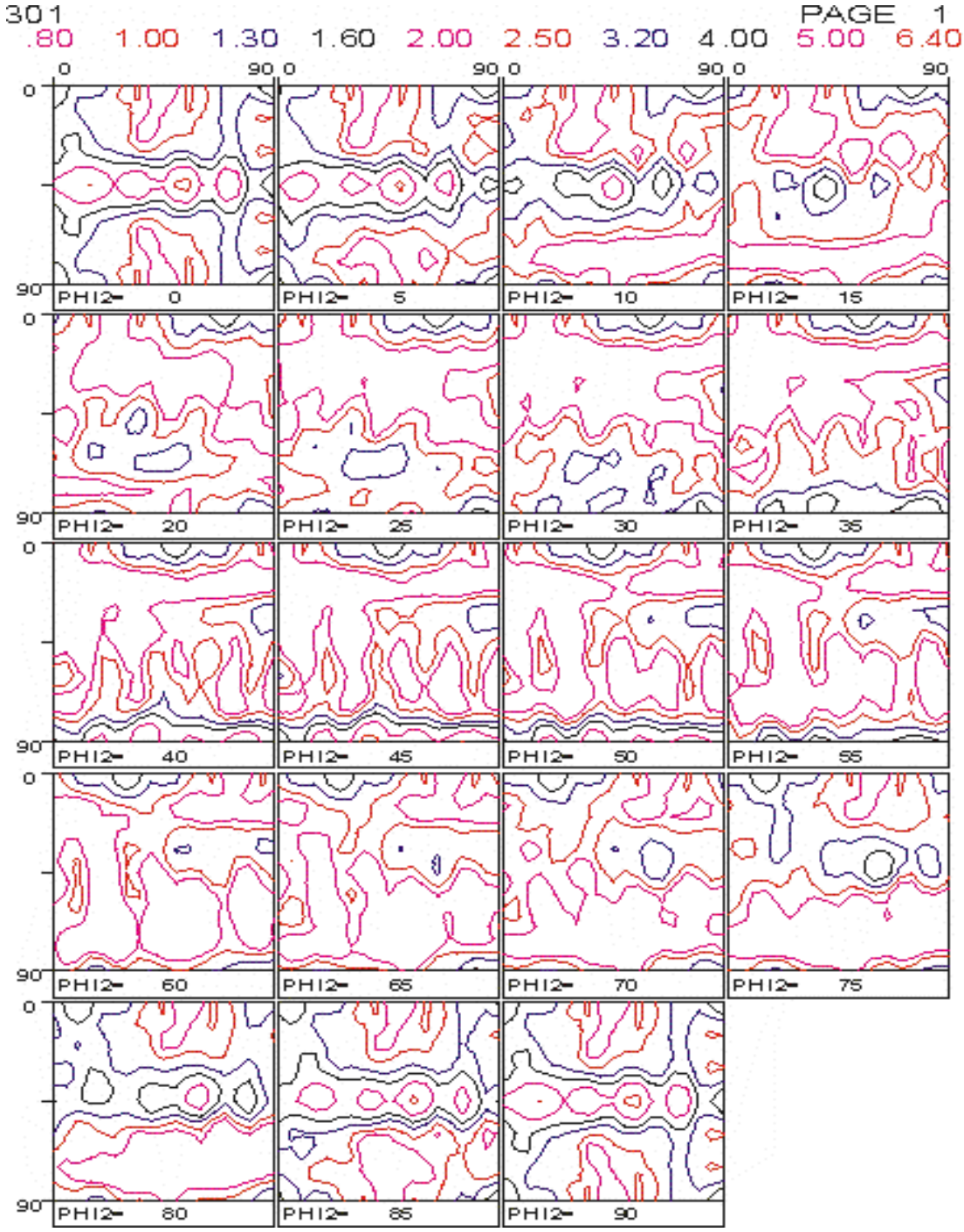

Figure 7a: ODF of SS 301 grade of Stainless Steel

The volume fractions of common texture components of the above texture components are shown in **Tables 3 & 4**. From the pole figures and ODFs, it is observed that varying fractions of different texture components exists in pole figures and ODFs for all FCC stainless steel sheets of different grades because they are of different composition. From the plots it is observed that the pole figures of the sheets of SS304 and SSLN1 show increased components of Taylor and 's' orientation. Even though's' and Taylor components are more, the recrystallized components (GOSS) is relatively more. Hence, the formability is expected to be better.

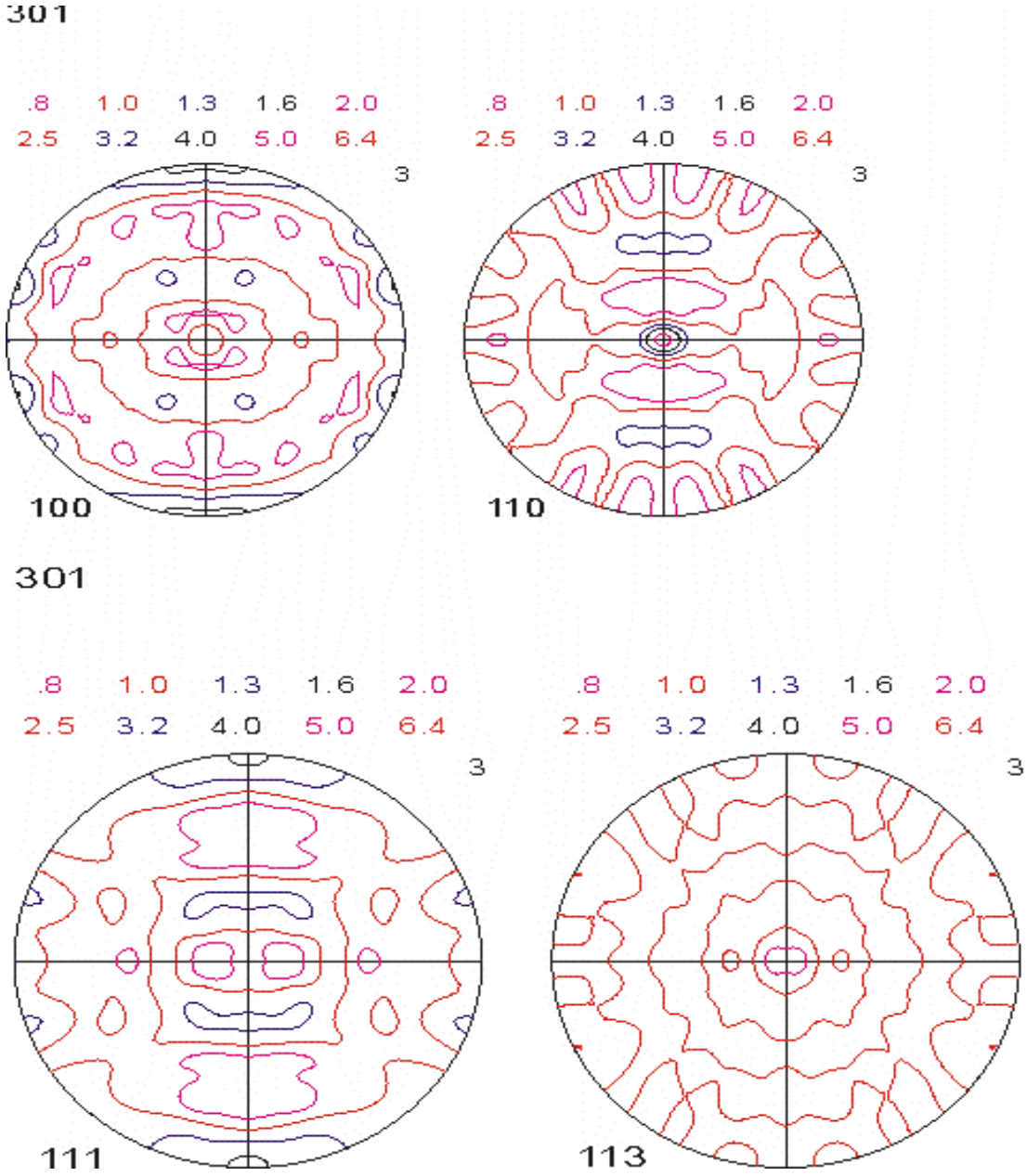

Figure 7b: Poles figures of SS 301 grade of Stainless Steel

Among all the steels, SS409M and SS430 exhibited fiber component, the ease of mechanical deformation is difficult and hence resulted in poor formability than SS304, SS301 and SSLN1. Between SS409M and SS430 steels SS409M exhibited poor formability, due to higher strength of α-fiber. The reason of developing fiber components in these two steels may be due to their BCC crystal structure. Martensitic structure of SS409M and austenitic structure of SS430 might have resulted in significant variation in formability.

Table 3: Volume fractions of texture components of SS 301, SS304 and SSLN1 (FCC)

Component symbol	Volume fractions		
	SS301	**SS304**	**SSLN1**
Cube	0.04	0.05	0.03
Taylor	0.08	0.10	0.13
Brass	0.10	0.12	0.12
S	0.18	0.21	0.25
Cu	0.09	0.11	0.13
CG	0.09	0.09	0.11
H	0.03	0.02	0.02
CH	0.07	0.06	0.05
Goss	0.05	0.05	0.07

Among three austenitic (FCC) base steels (SS301, SS304 and SSLN1), SS304 and SSLN1 steels exhibited better formability due to high Taylor and low 'H' component strengths. Even though, no large variation is observed in texture components between SS301 and other austenitic grade steels, the strong tendency for phase transformation could have resulted in restricted formability in SS301 than the other two.
Similarly the percentage of Cube and Brass components are high for SS304. The value in volume fraction of cube, brass and S components increase the formability[15], where as the copper component seems to play neutral role.

Table 4: Volume fractions of texture components of SS 430 and SS409 (BCC)

Component symbol	Volume fractions	
	SS409	**SS430**
Gamma	0.24	0.30
Alpha	0.33	0.31
F	0.11	0.14
F	0.12	0.14
H	0.06	0.04
I	0.12	0.13
Goss	0.03	0.07

Among these stainless steel sheets, SS304 shows the strong texture whose formability is higher. Similarly, the superior formability behaviour of SS304 stainless sheet metals is also justified by the tensile and formability properties recorded and presented in tensile properties table.

For the sheets of SS304 and SSLN1, the strain-hardening index value and the nR (strain-hardening index multiplied by the normal anisotropy value) values are found to be high which quantify the formability is greater when compared to the other sheets of various grades.

The formability of austenitic stainless steel grades is superior because of phase transformation during plastic deformation. The tensile and formability properties of SS304 sheet metals are found to be superior when compared to the rest of the stainless steel grades.

CONCLUSION

Following conclusions can be drawn from the above results and discussion:

1. A straightforward analysis is presented that relates void coalescence to the strain-hardening exponent and the factor within the inter-void ligament of the voids.
2. The hydrostatic strain or mean strain (e_m) cannot be related with d-factor and dd-factor because the fracture behaviour of austenitic stainless steel grades are different compared to other grades.
3. The Hydrostatic strain (e_m) also influences the void area fraction (Va) to great extent. The void area fraction (Va) is found to be higher for SS304 steel sheet due to the presence of lesser amount of carbides and sulphides and thus exhibits better formability and fracture strain than the rest of the sheets.
4. In addition to that, SS304 steel sheet shows lower L/W ratio and exhibits better formability and fracture strain. The formability of SSLN1 is comparable with SS304.
5. The higher value in volume fraction of Goss component indicates low formability which is high for SS430. The sheets of SS430 have lower nR-value which leads to inferior formability. On the other hand, SS304 and SSLN1 show better formability because of phase transformation during plastic deformation.

ACKNOWLEDGEMENT

The authors would like to thank M/s Salem Steel Plant, Steel Authority of India Limited (SAIL), Salem, Tamil Nadu, India for supplying the different stainless steel grades and Metallurgy group (Professor I. Samajdar), Indian Institute of Technology, Bombay, India for assistance in carrying out the texture study.

REFERENCES

[1] A.L. Gurson: J. Eng. Mater. Technol., "Continuum Theory of Ductile Rupture by Void Nucleation and Growth" Part I—Yield Criteria and Flow Rules for Porous Ductile Media, 1977, 99(1), 2-15.

[2] F. William, A. Hosford and John L. Duncan, "Sheet Metal Forming: A Review", JOM, 1999, 51 (11), 39-44.

[3] R. Narayanasamy and C. Sathiya Narayanan, " Some aspects on fracture limit diagram developed for different steel sheets", Materials Science and Engineering, A, 2006, 417; 197–224.

[4] A.A. Benzerga, J. Besson and A. Pineau, " Anisotropic ductile fracture: Part I: experiments" Acta Mater., 2004, 52, 4623–4638.

[5] A.R. Ragab and C. Saleh, "Effect of void growth on predicting forming limit strains for planar isotropic sheet metals", Mech. Mater., 1999, 32, 71 – 84

[6] X. Gao and J. Kim," Modeling of ductile fracture: Significance of void coalescence", Int. J. Solids Struct., 2006, 43, 6277–6293.

[7] J.P. Bandstra and D.A. Koss," Modeling the ductile fracture process of void coalescence by void-sheet formation", Materials Science and Engineering, A, 2001, 319–321; 490–495

[8] Z. Li, C. Wang and C. Chen, "The influence of matrix yield stress gradient on the growth and coalescence of spheroidal voids" Int. J. Solids Struct., 2002, 39(3), 601-616.

[9] A.R. Ragab, "Prediction of fracture limit curves in sheet metals using a void growth and coalescence model**",** J. Mater. Process. Technol., 2008, 199 (1-3), 206–213.

[10] V. Monchiet, C. Gruescu, E. Charkaluk and D. Kondo, "Approximate yield criteria for anisotropic metals with prolate or oblate voids", Comptes Rendus Mécanique, 2006, 334 (7), 431-439.

[11] C.F. Niordson, "Void growth to coalescence in a non-local material", Eur. J. Mech. A. Solids., 2008, 27(2), 222–233.

[12] Tvergaard. V and J.W. Hucthison: J. Appl. Mech., 1993, 60(4), 807-812.

[13] A. Kanni Raj and K.A. Padmanabhan: J. Mater. Process. Technol., 1999, 94(2-3); 201-207

[14] B. Hutchinson, L. Ryde, E. Lindh and K. Tagashira: Mater. Sci. Eng., A, 1998, 257(1); 9-17.

[15] M. Safaeirad, M.R. Toroghinejad and F. Ashrafizadeh: J. Mater. Process. Technol., 2008, 196(1-3); 205–212.

[16] I. Samajdar, B. Verlinden and P. Van Houtte: Acta Mater., 1998, 46(8), 2751-2763.

[17] I. Samajdar and R. D. Doherty: Acta Mater., 1998, 46(9), 3145-3158..

[18] J-H Han, J-Y. Suh, K-K. Jee and J-C. Lee: Mater. Sci. Eng., A, 2008, 477 (1-2), 107-120.

[19] R. Narayanasamy, N.L. Parthasarathi and C. Sathiya Narayanan: Materials & Design, 2009, 30(4), 1310-1324.

[20] R. Narayanasamy: Drawability of steel metals through conical and tractrix dies. Ph.D. Thesis, 1992, Department of Production Engineering, Regional Engineering College, Tiruchirappalli-620015, Tamil Nadu, India.

[21] Handbook of stainless steel fabrication, Allegheny Ludlum Steel Corporation, Pittsburgh, USA, 1960.